The Journal of Investigative Dermatology

Structural and functional analysis of intact hair follicles and pilosebaceous units by volumetric multispectral optoacoustic tomography

Journal:	*Journal of Investigative Dermatology*
Manuscript ID:	Draft
Manuscript Type:	
Date Submitted by the Author:	n/a
Complete List of Authors:	Ford, Steven; Helmholtz Zentrum München, Institute for Biological and Medical Imaging Sardella, Thomas; iThera Medical, GmbH, N/A Urich, Alexander; iThera Medical, GmbH, N/A Burton, Neal; iThera Medical, GmbH, N/A Kacprowicz, Marcin; iThera Medical, GmbH, N/A Bigliardi-Qi, Mei; Agency for Science, Technology and Research, Institute of Medical Biology; National University Hospital, University Medicine Cluster, Division of Rheumatology Olivo, Malini; Agency for Science, Technology and Research, Singapore Bioimaging Consortium Bigliardi, Paul; Agency for Science, Technology and Research, Institute of Medical Biology; National University Hospital, University Medicine Cluster, Division of Rheumatology Razansky, Daniel; Helmholtz Zentrum München, Institute for Biological and Medical Imaging; Technische Universität München, Faculty of Medicine
Key Words:	Pilosebaceous Unit, Optoacoustic Imaging, Hair Shaft, Dermal Papilla, Sebaceous Gland

Note: The following files were submitted by the author for peer review, but cannot be converted to PDF. You must view these files (e.g. movies) online.

Movie 1.avi

Structural and functional analysis of intact hair follicles and pilosebaceous units by volumetric multispectral optoacoustic tomography

Steven J. Ford[1], Thomas Sardella[2], Alexander Urich[2], Neal C. Burton[2], Marcin Kacprowicz[2], Mei Bigliardi[3,4], Malini Olivo[5*], Paul L. Bigliardi[3,4*], and Daniel Razansky[1,6*]

[1]Institute for Biological and Medical Imaging (IBMI), Helmholtz Zentrum München, Neuherberg, Germany

[2]iThera Medical GmbH, Munich, Germany

[3]Institute of Medical Biology, Agency for Science, Technology and Research, Singapore

[4]University Medicine Cluster, Division of Rheumatology, National University Hospital, Singapore

[5]Singapore Bioimaging Consortium, Agency for Science, Technology and Research, Singapore

[6]Faculty of Medicine, Technische Universität München, Munich, Germany

* Correspondence should be addressed to D.R. (dr@tum.de), M.O. (malini_olivo@sbic.a-star.edu.sg), or P.L.B. (paul.bigliardi@imb.a-star.edu.sg)

ABSTRACT (200 WORD LIMIT)

Visualizing anatomical and functional features of hair follicle development in their unperturbed environment is key in understanding complex mechanisms of hair patho-physiology and in discovery of novel therapies. Of particular interest is *in-vivo* visualization of the intact pilosebaceous unit, vascularization of the hair bulb and evaluation of the hair cycle. Furthermore, non-invasive visualization of the sebaceous glands could offer crucial insight into patho-physiology of follicle-related diseases, dry or seborrhoic skin, in particular by combining in-vivo imaging with other phenotyping, genotyping and microbial analyses. The available imaging techniques are limited in their ability for deep tissue in-vivo imaging of hair follicles and lipid-rich sebaceous glands in their entirety without biopsy. We developed a non-invasive, painless and risk-free volumetric multispectral optoacoustic tomography (vMSOT) method for deep tissue three-dimensional visualization of whole hair follicles and surrounding structures with high spatial resolution below 70µm. Herein we demonstrate on-the-fly assessment of key morphometric parameters of follicles and lipid content as well as functional oxygenation parameters of the associated capillary bed. The ease of handheld operation and versatility of the newly-developed approach poise it as an indispensable tool for early diagnosis of disorders of the pilosebaceous unit and surrounding structures, and for monitoring the efficacy of cosmetic and therapeutic interventions.

INTRODUCTION

Visualization of the entire viable hair follicle, including the pilosebaceous unit and papilla, is important for characterizing various types of follicular-related disorders, including hair loss (alopecia), acne, folliculitis, keratosis pilaris, and seborrheic or dry skin conditions. Follicular dysfunction is associated with a number of environmental and familial factors, yet our understanding of the mechanisms of such disorders remains limited. Alopecia, for example, occurs when abnormal cycling causes the hair follicle to permanently transition into the resting phase (telogen), never re-entering the growth phase (anagen). Inheritable alopecia is correlated with a number of abnormalities, including hormonal (e.g. androgenic, dihydrotestosterone (Sawaya and Price, 1997; Schweikert and Wilson, 1974)) and gene transcription factors (e.g. the Mediator coactivator (Oda *et al.*, 2012), SOX21 (Kiso *et al.*, 2009)), and other cell signaling pathways (Shh, Wnt, growth factors (Johnstone and Albert, 2002; Malkinson *et al.*, 1993)). However, still unclear is exactly how these and other underlying factors are linked to healthy or aberrant morphometry and cycling of the pilosebaceous unit and cause hair loss.

Real-time 3D *in-vivo* visualization of the entire, intact pilosebaceous unit would aide in understanding causes and consequences of various forms of alopecia and follicular diseases. *In-situ* measurements could provide new insights into the pathophysiology of these diseases by observing the hair follicles non-invasively over time, and to monitor the efficacy of respective pharmaceutical or cosmetic treatments. Current methods to examine intact hair follicle viability rely primarily on biopsies, which are unfavorable due to their invasiveness. In addition, fixation and staining solutions may also dehydrate the studied tissue slice and disrupt the overall structure of the pilosebaceous unit and the hair follicle cannot be used to study the evolution of a change

or disease over time. A standard biopsy gives us only one time point in the disease and non-invasive, morphological observation over time can add a new time dimension for accurate clinical evaluation. Current imaging methods are restricted by the optical diffusion limit (e.g. in-vivo reflectance confocal imaging and OCT), and also by the spatial resolution (e.g. Ultrasound or OCT), limiting the abilities of these methods to image pilosebaceous structures found at depth. Recent advances in multiphoton microscopy approaches allow for imaging of labeled follicular cells (Rompolas *et al.*, 2012), but visualization of the pilosebaceous unit is hindered by the effective imaging depth, in the range of hundreds of μm range due to strong light scattering in living tissues.

The imaging depth limitation of optical microscopy related to light scattering in living tissues can be generally overcome by means of optoacoustic techniques (Razansky *et al.*, 2012). By detecting pressure waves induced via transient absorption of short high-energy laser pulses, optoacoustic methods have recently enabled high-resolution imaging with optical contrast at depths of several millimeters to centimeters (Razansky, 2012; Razansky *et al.*, 2009a; Yao and Wang, 2014), orders of magnitude deeper than possible with modern microscopy. The ability to spatially resolve spectral information (i.e., location/size of unique tissue structures containing specific chromophores) provides added advantage of optoacoustic techniques; multispectral imaging (i.e. images taken at multiple excitation wavelengths) and unmixing allows for visualization of intrinsic tissue chromophores, such as melanin (Krumholz *et al.*, 2011), oxy and de-oxy hemoglobin (Laufer *et al.*, 2007; Wang *et al.*, 2003), lipids and water. The potential of multispectral optoacoustic tomography for functional and molecular imaging is highlighted by the broad range of biological applications, including cardiovascular imaging (Taruttis *et al.*, 2010; Taruttis *et al.*, 2013), monitoring of organ perfusion and pharmacokinetics (Razansky *et*

al., 2011; Taruttis *et al.*, 2012), targeted studies of inflammation and arthritis (Beziere *et al.*, 2014; Fournelle *et al.*, 2012; Vonnemann *et al.*, 2014), neuroimaging (Wang *et al.*, 2003; Wang *et al.*, 2006) and skin imaging (Ida *et al.*, 2014; Schwarz *et al.*, 2014; Vionnet *et al.*, 2014). In the present study, we imaged human hair follicles and resolved intrinsic absorbers such as melanin, hemoglobin, and lipid structures in their natural intact environment *in-vivo* by means of high-resolution volumetric multispectral optoacoustic tomography (vMSOT). Our finding suggest that vMSOT has high potential for clinical and research applications, from which the link between morphologies of intact pilosebaceous structures and molecular mechanisms can be explored.

RESULTS

Anatomical features as identified in single-wavelength images

Fig 1A shows a schematic of the imaging system and a representative 3D optoacoustic image of a small cluster of hair follicles on the scalp is further shown in Fig 1B. The entire hair follicle, which extends towards the skin surface from deep within the tissue, can be readily identified in the image. Important morphometric features, such as hair follicle length, were subsequently determined, allowing for a distinction of phases of growth for each hair follicle. Hairs marked '1' and '2' in Fig 1B had measured shaft lengths of about 3 mm and uniform structure, suggesting that this hair was in the normal growth phase (anagen). Conversely, the hair marked '3' had a measured shaft length of approximately 2 mm and the dermal papilla appeared detached from the hair shaft, indicating that this hair may be in the transition or resting phases (catagen or telogen). For comparison, Fig 1C shows corresponding structures as they appear on

a typical histological Masson's Trichrome staining of a normal scalp biopsy. The effective penetration depth of our imaging method can be determined from the images as the deepest resolvable structure in the reconstructed 3D volume. This structure was a branch of the large vessel identified in Fig 1B, determined to be ~4.7 mm below the skin surface (indicated by a blue dashed line in Fig 1B).

The accompanying video available in the online version of the manuscript (Movie 1) further presents maximal intensity projection (MIP) views recorded at a single wavelength of 850nm at a frame rate of 20 volumes per second. For this, the probe was scanned across a small region of ~10mm on the forehead, starting at the hairline, moving to the scalp, and coming back to the hairline while also focusing on visualization of vessels.

Multispectral unmixing for specific chromophores

Linear spectral unmixing of optoacoustic images acquired at multiple wavelengths (see complementary methods for details) further enhanced specificity in detecting various tissue chromophores in the pilosebaceous unit by using their known absorption profiles (shown in Fig 2A). Results from the linear unmixing of a single hair follicle are shown in Fig 2B, allowing for a unique and robust separation of the unmixed chromophores. The structures of the same single pilosebaceous unit on the scalp are shown in detail in Fig 3, while unmixing results of a cluster of pilosebaceous units on the hand is further shown in detail in Fig 4. Thus, several key structural components of the pilosebaceous units were delineated by the unmixing method, making possible the visualization of blood perfusion (i.e., unmixed hemoglobin signal) in the

dermal papilla, surrounding dermis and subcutaneous tissue, as well as evaluation of the relative level of blood oxygenation in these structures. In addition, spectrally unmixed images allowed for structural analyses of the dermal papilla, and lipid- and melanin-rich structures surrounding the hair follicle.

Oxygenation of root capillary bed

As indicated in Fig 3, the root structure of the hair follicle on the scalp showed a point of high oxyhemoglobin signal, as was consistent across all the scans taken from the scalp (data not shown). This suggests that the dermal papilla is highly perfused, thus likely to be in the healthy growth (anagen) phase. The relative oxygenation (sO_2) of hemoglobin around the dermal papilla was estimated for this particular hair follicle to be approximately 99%.

Volume analysis of lipid structures

Unmixed images revealed an elliptical structure displaying a strong lipid signal near a hair follicle imaged on the scalp (Fig 3). Major and minor axes of the ellipsoid were estimated to be 4.3, 2.5, and 3.4 mm, which gave an overall lipid volume of 153 μL. Due to its superficial location around the hair follicle, much of this lipid signal could be linked to a network sebaceous glands. The lipid structures identified in the hand (Fig 4) were more dispersed and might correlate to lipids from both the sebaceous glands and subcutaneous fat.

Volume analysis of entire hair follicle

The melanin components of the unmixed images were used to assess hair follicle root dimensions. The length of the hair follicles were longer on the scalp than on the hand ($P < 0.05$), measuring approximately 3.16 ± 0.056 mm on the head (Fig 3), as compared to 2.19 ± 0.233 mm on the hand (Fig 4). Likewise, the volumes of the hair shaft and bulb follicles were greater on the scalp ($P < 0.05$), measuring approximately 0.278 ± 0.056 mm^3 on the head (Fig 3), as compared to 0.089 ± 0.033 mm^3 on the hand (Fig 4). The thicknesses of the entire hair follicles were also determined on both the scalp (Fig 5A) and the hand (Fig 5B), along the depth of each hair. In general, hair was thicker on the scalp as compared to the hand ($P < 0.05$), and all hairs were thickest at the level of the hair bulb and papilla and became thinner towards the skin surface. These findings fit well with what is expected, since hairs on scalp are much longer and thicker and the hair bulbs are deeper located compared to corporal hairs (e.g., the hand).

Visualization of pores

Small, round, superficial structures, corresponding to the locations of follicular openings (ostium), were observed in optoacoustic images acquired from the forehead of a subject (Fig 6A). These structures displayed particular prominence at shorter wavelengths, but generally diminished in signal strength and the shape as wavelength increased. The absorbance of these structures decreased as illumination wavelength increased, but also displayed a peak in absorbance at approximately 1200 nm (Fig 6B). The peak at approximately 1200 nm spectrum suggests that these structures comprise lipids, yet the spectrum was distinct from any of tissue chromophores accounted for so far in the unmixing algorithm. This indicates the presence of

other tissue chromophore(s), possibly porphyrins, proteins produced by the skin bacteria (e.g., *p. acnes*), which is known to feed on fatty acids and sebum.

DISCUSSION

We report here a novel technique to measure structural and physiological features of intact hair follicles using a handheld volumetric multispectral optoacoustic tomography (vMSOT). This new imaging paradigm allows for high resolution, label-free 3D visualization of the structures of the pilosebaceous unit at imaging depths of several millimeters and beyond, an order of magnitude greater than what can be achieved with advanced microscopy methods. Single-wavelength images allowed for determination of the phase (anagen, telogen/catagen) and structural information of intact pilosebaceous units, illustrating the potential for vMSOT to evaluate key morphometric parameters of the hair follicle. Structures observed by vMSOT agree well with what is expected in a histological slice (Fig 1C) and biopsy of the pilosebaceous unit (Jimenez *et al.*, 2011). Of interest is that, due to the 2D nature of conventional histology, slices cannot distinguish the phase of hair growth as readily as our technique. In addition, vMSOT does not require extraction of the follicular unit, allowing for monitoring of the morphology and phase of a single intact hair follicle growth over several growth cycles. Morphological information of the intact follicle would be of high value in longitudinal studies of hair pathophysiology and the response of the hair follicle cycle to environmental factors (e.g. chemotherapy). The fully non-invasive visualization can aide in the development of treatments for hair loss and evaluations of preventative measures to reduce or avoid hair loss by monitoring the efficacy of potential therapeutic agents on a given hair follicle or cluster of follicles. In

addition, this method can be useful in linking the growth phase of the hair follicle molecular mechanisms, since the morphological features can be assessed by vMSOT immediately prior to follicular unit extraction for immunohistochemical and molecular biology evaluation. For instance, hair follicles in aberrant growth can be selected for further assessment (e.g., RNA/DNA sequencing) and accurately identified in a specific growth phase for robust correlation of morphology and biology.

Unmixing of tissue chromophores increased the specificity in visualizing key features, including melanin-containing structures (e.g., moles, hair bulb and shafts), as well as lipid-containing structures (e.g., sebaceous glands and/or subcutaneous fat). The unmixed melanin component showed relatively high signal in the hair follicle when compared to the skin and surrounding tissue of the epidermis. While somewhat surprising, the high contrast between the follicle structure and skin is likely due to the relatively high concentration of melanin in the hair compared to keratinocytes in the skin. This high contrast in the contribution of melanin enabled unique estimations of the dimensions and pigmentation of a given hair shaft, valuable parameters particularly for researchers studying alopecia and treatments thereof. In addition, the volumes of lipid-rich structures such as sebaceous glands can be measured, important parameters to characterize disease related changes (e.g., acne or folliculitis) of the pilosebaceous unit and to evaluate efficacy of therapeutic agents for such diseases. Lipid content produced by the sebaceous glands of the pilosebaceous units is important for follicular health (Zouboulis *et al.*, 2014), known to have a unique composition of fatty acids in normal sebum analytes (Zouboulis *et al.*, 2008). This information will be useful in future experiments aimed at determining the absorption spectrum of sebum in order to allow for multispectral unmixing of sebum from fat by

vMSOT. Other approaches, such as frame averaging, application of advanced unmixing algorithms, and refined wavelength selection could further enhance our ability to accurately unmix the sebaceous glands and sebum in future experiments. The multispectral approach further allowed for estimating multiple physiological parameters, including perfusion and blood oxygenation of the follicle bulb and the surrounding capillary bed. Perfusion and relative oxygenation are viewed as important potential markers which may reveal additional causes of various forms of hair loss, and help characterize the efficacies of potential therapies. For instance, the supply of blood to the follicle is an important factor in the normal phasic cycling (Stenn and Paus, 2001). Furthermore, follicular diseases related to limited vascular perfusion could be possibly revealed and further characterized using vMSOT.

Another unique finding was that vMSOT was capable of resolving small, pore-like structures where hairs were presumably below the resolution limit and thus too small to be seen (Fig 6). These structures showed two absorbance peaks; one at low wavelengths, presumably peaking at a wavelength below the system limit of 660 nm, and one at approximately 1210 nm. The peak at 1210 nm suggests these structures are lipid-rich in nature, whereas the peak at lower wavelengths suggests that another chromophore other than melanin and hemoglobin is present. One likely candidate chromophore is assumed to be protoporphyrin IX, an intrinsic chromophore produced by the skin bacteria p. acnes (Konig *et al.*, 2000). The unique absorption profile may also be a result of protoporphyrin IX and altered lipids (oxidation or metabolization by surface microbiome) from sebaceous glands with different absorption spectra than the lipids in the sebaceous glands described in Figure 3. Future experiments that could measure the absorption spectra of *p. acnes* at the system-specific wavelengths will allow for further unmixing and

identification of sebaceous units affected by acne. With such information, vMSOT could potentially diagnose skin-borne pathogens by characterizing the particular absorbance spectra for given pathogens based on the expression of intrinsic chromophores, such as the porphyrins and chlorophylls expressed by *p. acnes* or *p. aeruginosa*.

In conclusion, these studies highlight the capabilities of optoacoustic imaging in visualizing the pilosebaceous unit and hair follicle structure. Robust physiological parameters offered by analysis of the real-time vMSOT data are expected to be useful in future studies to determine the underlying mechanisms of hair loss and treatments of respective diseases. Parameters related to perfusion (i.e. sO_2) and root structure (i.e. length, volume) can be readily used as an indication of whether the follicle is in growth or dormancy phases and thus can assess efficacy of potential treatments for alopecia. Refinement of lipid unmixing will further allow for the determination of whether a disease or treatment impacts sebaceous gland function. Collectively, these findings offer a novel approach in characterizing the structure and status of the pilosebaceous unit and studies of potential treatments.

MATERIALS AND METHODS

Experimental system

An illustration of the handheld system components is shown in Fig 1A. Healthy volunteers were imaged on the head or hand, where hairs were shaved prior to the imaging session. Optoacoustic signals were generated in the scalp or hand of healthy volunteers using a pulsed laser system

capable of generating nanosecond pulses at a rate of up to 100Hz and fast wavelength tuning in the range between 660-1300 nm on a per-pulse basis (Innolas Laser GmbH, Krailling, Germany). The excitation light was delivered to the target regions by means of a fiber bundle. The resulting optoacoustic responses were measured using a custom-made handheld matrix ultrasound detection array, which consisted of 512 detection elements arranged in a semi-spherical geometry covering a solid angle of approximately 140 degrees (Imasonic, Voray-sur-l'Ognon, France). The individual elements provided broad detection bandwidth of 70% around the central frequency of 10 MHz, corresponding to diffraction-limited spatial resolution of 75µm. Data was acquired using a custom-built data acquisition unit (DAQ, Falkenstein Mikrosysteme GmbH, Taufkirchen, Germany), which is triggered by the laser pulses and simultaneously samples signals from the individual detection elements at a rate of 40 megasamples per second. Uniform ultrasound coupling between the sample and detector was provided by filling a custom-made coupling chamber which housed gas-free water (H_2O) for hair imaging without lipid unmixing or heavy water (D_2O) for hair imaging including lipid unmixing. A thin, optically and acoustically transparent, water-tight polyethylene membrane was fixed to the edges of the coupling chamber, allowing for easy replacement and sterile use between imaging sessions.

Data processing

Image reconstruction was performed using a three-dimensional backprojection algorithm, as described in detail elsewhere (Xu and Wang, 2005). Optoacoustic signals were used to reconstruct images within a volume of 7.5 * 7.5 mm and 9 mm depth with an isotropic resolution of 75 µm per voxel. Reconstruction was implemented on a GPU (Dean-Ben *et al.*, 2013),

allowing for near-video rate volumetric image rendering at up to 20 Hz. A representative 3D optoacoustic image acquired from the scalp is shown in Fig 1B.

Linear unmixing of multispectral images revealed the spatial distribution of the various tissue chromophores (Razansky *et al.*, 2009a; Razansky *et al.*, 2009b; Razansky *et al.*, 2007). For this, volumetric images were acquired at several wavelengths correlating to key spectral features of the chromophores expected within the imaged tissue. In this study, we assumed the following chromophores to have significant contributions to light absorption in the wavelength range supported by the laser: hemoglobin, oxyhemoglobin, lipid, melanin, and water. Distribution of the chromophores was subsequently retrieved by spectral processing of optoacoustic images obtained at the various illumination wavelengths. Linear least square fitting (LSQ) unmixing was applied on a per voxel basis using the known molar extinction coefficient spectra of the chromophores of interest (Fig 2A). The lipid spectrum was determined analytically, based on the results by Nachabe et al. (Nachabe *et al.*, 2011).

Determination of physiological parameters

Following spectral unmixing, further analysis of the components was performed to determine key physiological parameters including lipid and hair follicle volume, and relative oxygenation of the capillary beds feeding the hair follicle root. The relative oxygenation of the blood vessels feeding the follicle bulb was calculated as the ratio of the oxyhemoglobin by total hemoglobin content (Laufer *et al.*, 2007; Wang *et al.*, 2006), i.e.

$$sO2 = \frac{AU_{HbO2}}{AU_{Hb} + AU_{HbO2}}$$

Due to the apparent elliptical shape of the resolved lipid structures, an ellipsoid was hand-fitted in order to determine lipid volume. Major and minor ellipsoid axes were determined from the lipid component of the unmixed image, which were then used to estimate the volume. Hair follicle root volume was determined by 3D segmentation of the individual hairs using Amira (FEI Visualization Sciences Group, USA). The lengths and volumes of the segmented hairs were subsequently calculated. Data are then expressed as mean ± standard deviation, and a two-tailed unpaired t-test was used to determine statistical difference of hair dimensions measured on the head and on the hand.

CONFLICT OF INTEREST

T.S., A.U., N.C.B., and M.K. are employees of iThera Medical, GmbH. ASTAR signed a Research Collaboration Agreement with iThera Medical without direct financial interests.

ACKNOWLEDGMENTS

D.R. recognizes funding from the European Union Research Council under grant agreement ERC-2010-StG-260991. M.O. and P.B. recognize funding from the Agency for Science, Technology and Research, in particular Institute of Medical Biology and Singapore Bioimaging Consortium. The HE slide from the scalp hair was generously provided by Dr. Graham Wright and Declan Lunny, from IMB, ASTAR.

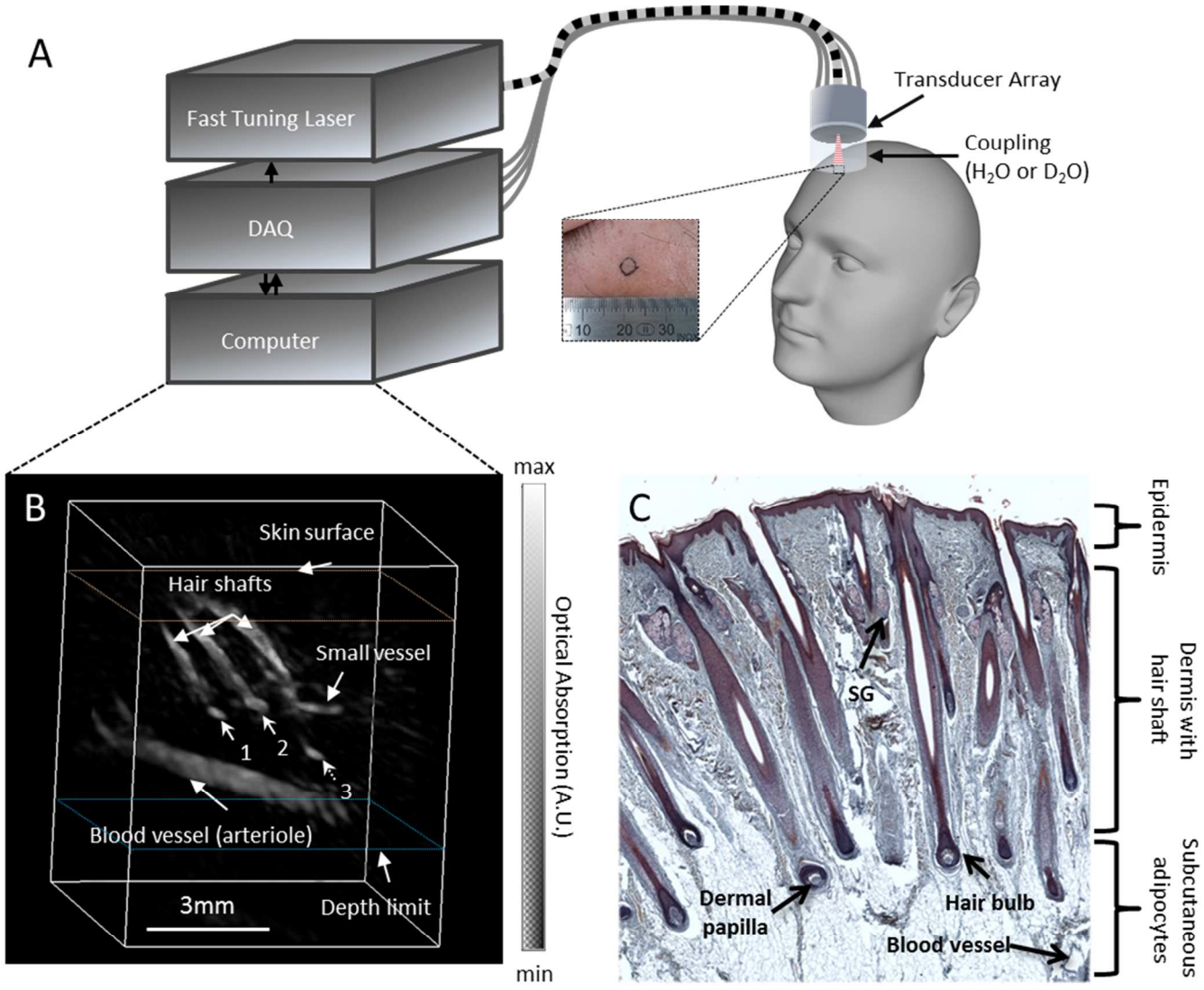

Figure 1: Handheld optoacoustic probe for high resolution real-time imaging of hair follicles. (A) Schematic of the imaging system and approach. The subject is imaged using a 512-element semi-spherical detector array that captures three-dimensional multispectral optoacoustic data in real time. The region of interest is illuminated using a pulsed OPO laser capable of fast wavelength tuning in an extended range 660-1300 nm at a rate of up to 100 Hz. The data acquisition unit (DAQ) simultaneously digitizes the optoacoustic signals, which are subsequently processed using a GPU-accelerated image reconstruction code to render 3D images for each laser shot. (B) Representative 3D optoacoustic image, demonstrating general physiological structures

below the skin surface, including the hair shafts and bulbs, dermal papilla (indicated by numbered arrows), and a deeper, larger blood vessel. The dermal papilla appear to be detached in hairs marked by arrow 3, suggesting this follicle may be in the catagen or telogen phase, whereas the dermal papillae of the hairs marked by arrows 1and 2 appear to be attached, suggesting these follicles are in an anagen phase. (C) Representative Masson's Trichrome microscope image (at 10x magnification) from paraffin embedded scalp hair of a healthy individual. When compared with the optoacoustic images, it reveals similar structures, namely, the dermal papilla, hair shafts and bulbs, and a large subcutaneous blood vessel. The hair bulbs and dermal papilla are located at some places in the subcutaneous fat tissue. Note that also visible in the histological image are sebaceous glands (SG) in the dermis close to the skin surface.

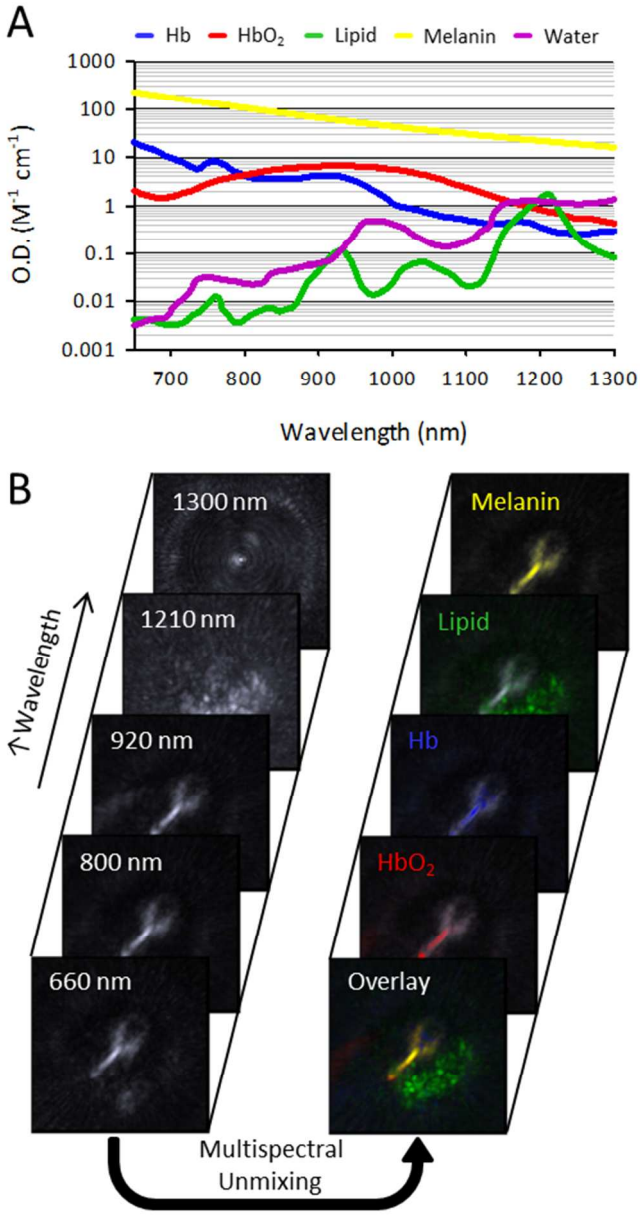

Figure 2: The multispectral imaging approach. (A) Images are collected at a range of wavelengths, chosen based on the shown absorption profiles of the chromophores of interest. (B) Optoacoustic images acquired at the multiple wavelengths allow for a linear unmixing of the data on a per-voxel basis and accurate mapping and quantification of the relative contribution of each chromophore.

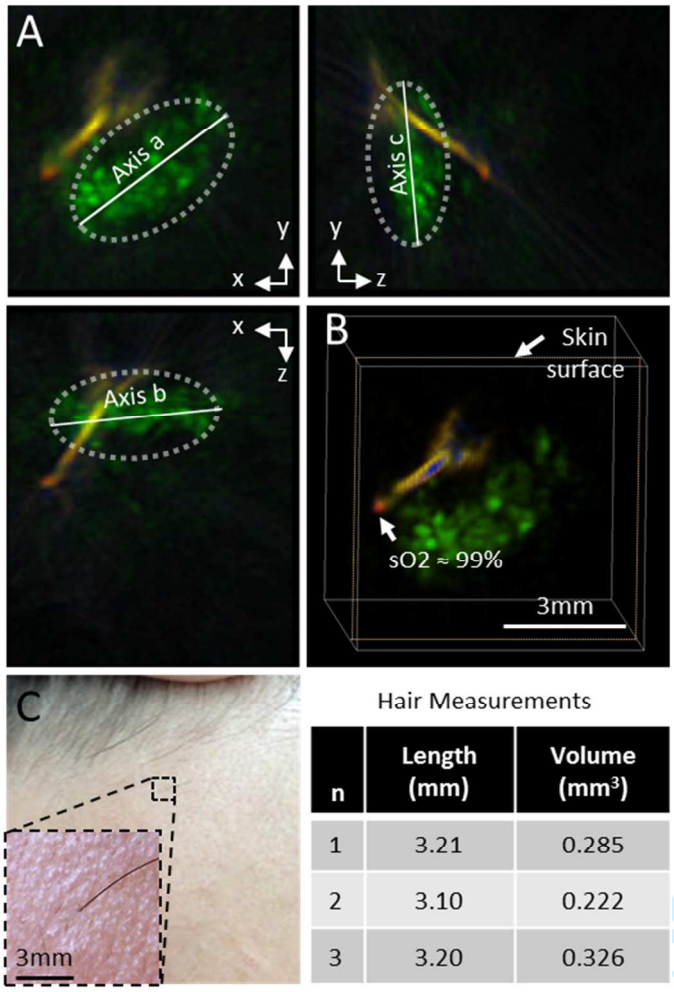

Hair Measurements

n	Length (mm)	Volume (mm^3)
1	3.21	0.285
2	3.10	0.222
3	3.20	0.326

Figure 3: Single pilosebaceous unit imaged on the forehead. (A) Unmixed images of a single hair on the scalp of a healthy volunteer. Multispectral unmixing allowed for the visualization of the single hair at depth, and also revealed an ellipsoid-like lipid structure near the follicle root. The dimensions of the lipid content were calculated along three axes shown in the orthogonal view in panel A (a = 4.3 mm, b = 2.5 mm, c = 3.4 mm). Assuming an elliptical shape, the estimated volume of the lipid structure was calculated to be 153 µL. (B) 3D representation of the unmixed data. (C) Photograph as well as a high-resolution micrograph (inlay) of the hair imaged, prior to shaving the hair. The length and volume of the hair shaft and bulb was measured from three separate scans, as quantified in the inlaid table. Of particular interest is that

the follicle bulb shows a high level of oxygenation, presumably corresponding to the highly-oxygenated capillary bed feeding the follicle. Colors reflect the contribution of each of the unmixed chromophores as follows: grey – OA signal at 800 nm; blue – deoxy hemoglobin; red – oxyhemoglobin; green – lipid; yellow – melanin.

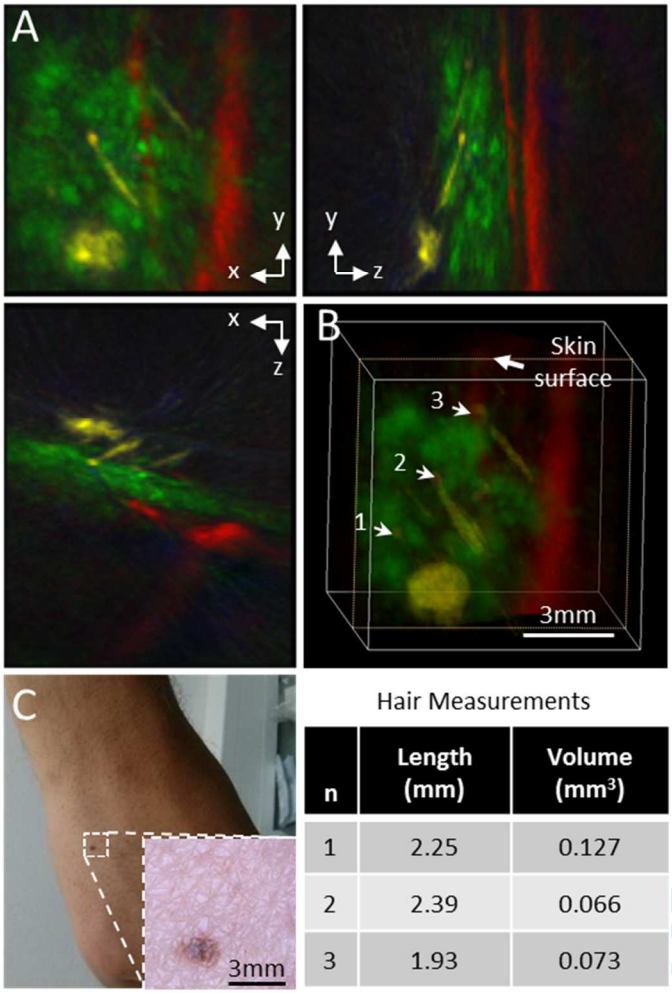

Hair Measurements

n	Length (mm)	Volume (mm^3)
1	2.25	0.127
2	2.39	0.066
3	1.93	0.073

Figure 4: A cluster of pilosebaceous units imaged on the hand. (A) The unmixed images of a hand in a region where both a mole (melanocyte deposit) and hairs are seen. The unmixed signal shows a strong lipid content, as well as strong melanin content, correlating to melanin concentrated in the hairs and mole. The lipid content was dispersed around the hairs deep under the skin surface, as can be seen in the orthogonal and 3D views of the hair. (B) Volumetric representation of the unmixed data. (C) Photograph, as well as a high-resolution micrograph (inlay) of the region, mole, and hairs imaged, after shaving the hairs. Measures of the length and volume of each of the three hairs visualized in this scan are tabulated in the inlaid table. Colors

reflect the contribution of each of the unmixed chromophores as follows: grey – OA signal at 800 nm; blue – deoxy hemoglobin; red – oxyhemoglobin; green – lipid; yellow – melanin.

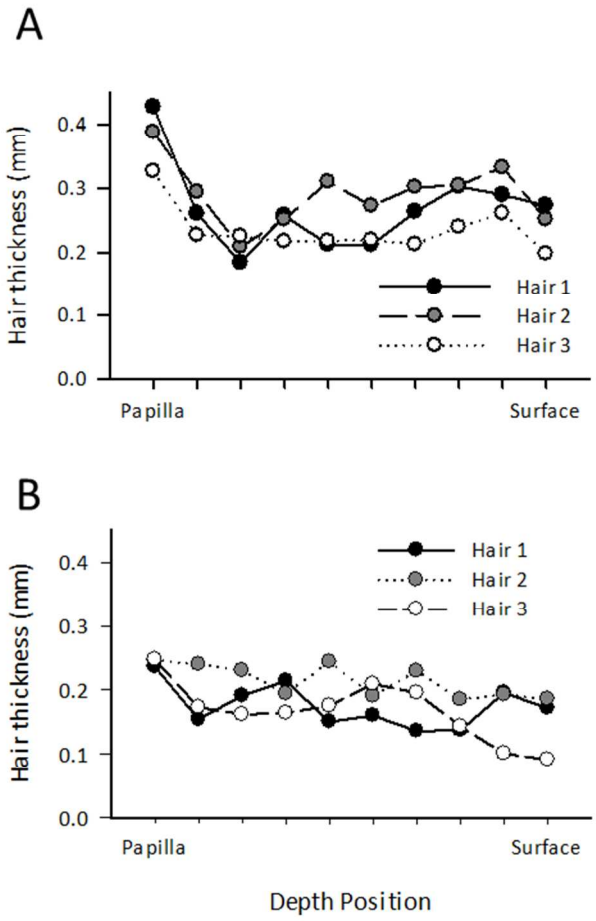

Figure 5: Measurements of hair shaft thickness at 10 different depths starting at the dermal papilla and ending at the skin surface. (A) Hair thicknesses measured on the scalp, which correspond to hairs 1, 2, and 3 of Fig 1B. (B) Hair thicknesses measured on the hand, corresponding to hairs 1, 2, and 3 of Fig 3B.

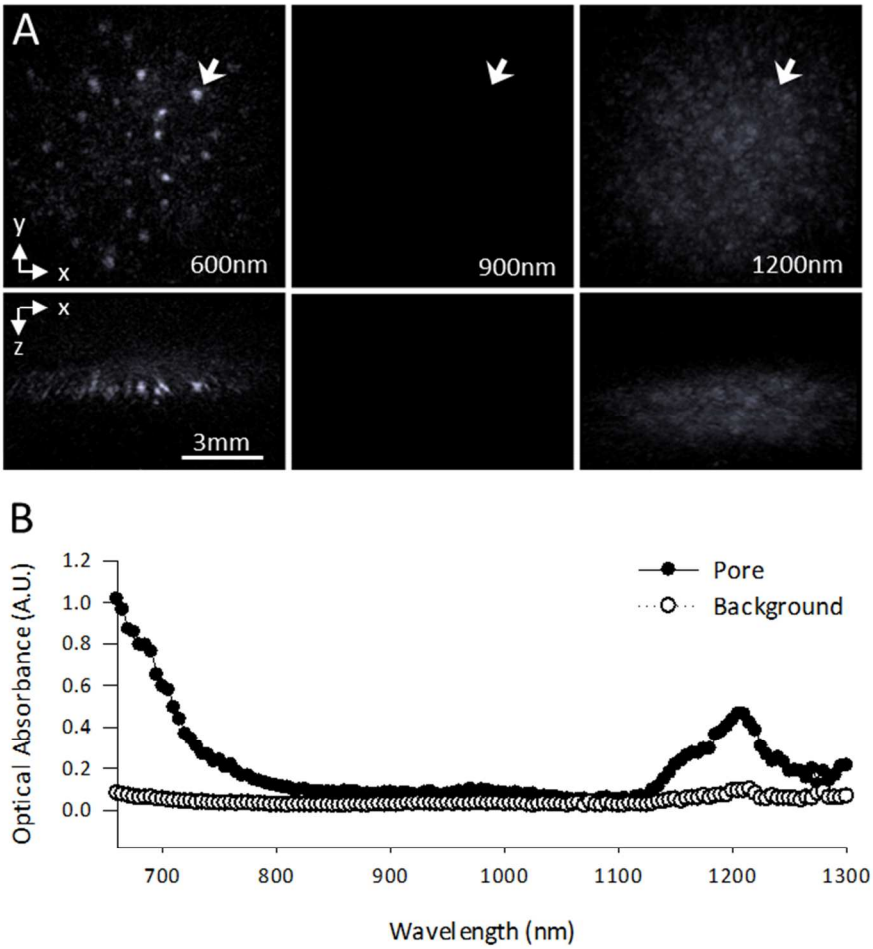

Figure 6: Multi-wavelength imaging of pigmented pores on the forehead of a volunteer. (A) Several highly-absorbing spherically-shaped objects are clearly identified near the skin surface at the shorter wavelengths, for example in image taken at 660 nm. These structures attenuate and eventually disappear at higher wavelengths. (B) The absorption spectrum of a given pore-like structure, as indicated by an arrow in panel A. This spectrum shows some similarity to the known absorbance spectra of porphyrin IX produced by the bacteria *p. acnes* or it could represent a mixture of microbial chromophores with sebaceous gland lipids altered by oxidation or microbial metabolism.

REFERENCES

Beziere N, von Schacky C, Kosanke Y, *et al.* (2014) Optoacoustic imaging and staging of inflammation in a murine model of arthritis. *Arthritis & rheumatology (Hoboken, NJ)* 66:2071-8.

Dean-Ben XL, Ozbek A, Razansky D (2013) Volumetric real-time tracking of peripheral human vasculature with GPU-accelerated three-dimensional optoacoustic tomography. *IEEE transactions on medical imaging* 32:2050-5.

Fournelle M, Bost W, Tarner IH, *et al.* (2012) Antitumor necrosis factor-α antibody-coupled gold nanorods as nanoprobes for molecular optoacoustic imaging in arthritis. *Nanomedicine : nanotechnology, biology, and medicine* 8:346-54.

Ida T, Kawaguchi Y, Kawauchi S, *et al.* (2014) Real-time photoacoustic imaging system for burn diagnosis. *J Biomed Opt* 19:086013.

Jimenez F, Izeta A, Poblet E (2011) Morphometric analysis of the human scalp hair follicle: practical implications for the hair transplant surgeon and hair regeneration studies. *Dermatologic surgery : official publication for American Society for Dermatologic Surgery [et al]* 37:58-64.

Johnstone MA, Albert DM (2002) Prostaglandin-induced hair growth. *Survey of ophthalmology* 47 Suppl 1:202.

Kiso M, Tanaka S, Saba R, *et al.* (2009) The disruption of Sox21-mediated hair shaft cuticle differentiation causes cyclic alopecia in mice. *Proceedings of the National Academy of Sciences of the United States of America* 106:9292-7.

Konig K, Teschke M, Sigusch B, *et al.* (2000) Red light kills bacteria via photodynamic action. *Cellular and molecular biology* 46:1297-303.

Krumholz A, Vanvickle-Chavez SJ, Yao J, *et al.* (2011) Photoacoustic microscopy of tyrosinase reporter gene in vivo. *Journal of biomedical optics* 16:80503.

Laufer J, Delpy D, Elwell C, *et al.* (2007) Quantitative spatially resolved measurement of tissue chromophore concentrations using photoacoustic spectroscopy: application to the measurement of blood oxygenation and haemoglobin concentration. *Phys Med Biol* 52:141-68.

Malkinson FD, Geng L, Hanson WR (1993) Prostaglandins protect against murine hair injury produced by ionizing radiation or doxorubicin. *The Journal of investigative dermatology* 101.

Nachabe R, Evers DJ, Hendriks BH, *et al.* (2011) Effect of bile absorption coefficients on the estimation of liver tissue optical properties and related implications in discriminating healthy and tumorous samples. *Biomed Opt Express* 2:600-14.

Oda Y, Hu L, Bul V, *et al.* (2012) Coactivator MED1 ablation in keratinocytes results in hair-cycling defects and epidermal alterations. *The Journal of investigative dermatology* 132:1075-83.

Razansky D (2012) Multispectral Optoacoustic Tomography-Volumetric Color Hearing in Real Time. *IEEE J Sel Top Quantum Electron* 18:1234-43.

Razansky D, Baeten J, Ntziachristos V (2009a) Sensitivity of molecular target detection by multispectral optoacoustic tomography (MSOT). *Medical physics* 36:939-45.

Razansky D, Buehler A, Ntziachristos V (2011) Volumetric real-time multispectral optoacoustic tomography of biomarkers. *Nature protocols* 6:1121-9.

Razansky D, Deliolanis NC, Vinegoni C, *et al.* (2012) Deep Tissue Optical and Optoacoustic Molecular Imaging Technologies for Pre-Clinical Research and Drug Discovery. *Curr Pharm Biotechno* 13:504-22.

Razansky D, Distel M, Vinegoni C, *et al.* (2009b) Multispectral opto-acoustic tomography of deep-seated fluorescent proteins in vivo. *Nature Photonics* 3:412-7.

Razansky D, Vinegoni C, Ntziachristos V (2007) Multispectral photoacoustic imaging of fluorochromes in small animals. *Optics letters* 32:2891-3.

Rompolas P, Deschene ER, Zito G, *et al.* (2012) Live imaging of stem cell and progeny behaviour in physiological hair-follicle regeneration. *Nature* 487:496-9.

Sawaya ME, Price VH (1997) Different levels of 5alpha-reductase type I and II, aromatase, and androgen receptor in hair follicles of women and men with androgenetic alopecia. *The Journal of investigative dermatology* 109:296-300.

Schwarz M, Omar M, Buehler A, *et al.* (2014) Implications of Ultrasound Frequency in Optoacoustic Mesoscopy of the Skin. *IEEE transactions on medical imaging*.

Schweikert HU, Wilson JD (1974) Regulation of human hair growth by steroid hormones. I. Testerone metabolism in isolated hairs. *The Journal of clinical endocrinology and metabolism* 38:811-9.

Stenn KS, Paus R (2001) Controls of hair follicle cycling. *Physiological reviews* 81:449-94.

Taruttis A, Herzog E, Razansky D, *et al.* (2010) Real-time imaging of cardiovascular dynamics and circulating gold nanorods with multispectral optoacoustic tomography. *Optics express* 18:19592-602.

Taruttis A, Morscher S, Burton NC, *et al.* (2012) Fast multispectral optoacoustic tomography (MSOT) for dynamic imaging of pharmacokinetics and biodistribution in multiple organs. *PloS one* 7.

Taruttis A, Wildgruber M, Kosanke K, *et al.* (2013) Multispectral optoacoustic tomography of myocardial infarction. *Photoacoustics* 1:3-8.

Vionnet L, Gateau J, Schwarz M, *et al.* (2014) 24-MHz scanner for optoacoustic imaging of skin and burn. *IEEE transactions on medical imaging* 33:535-45.

Vonnemann J, Beziere N, Böttcher C, *et al.* (2014) Polyglycerolsulfate functionalized gold nanorods as optoacoustic signal nanoamplifiers for in vivo bioimaging of rheumatoid arthritis. *Theranostics* 4:629-41.

Wang X, Pang Y, Ku G, *et al.* (2003) Noninvasive laser-induced photoacoustic tomography for structural and functional in vivo imaging of the brain. *Nat Biotechnol* 21:803-6.

Wang X, Xie X, Ku G, *et al.* (2006) Noninvasive imaging of hemoglobin concentration and oxygenation in the rat brain using high-resolution photoacoustic tomography. *Journal of biomedical optics* 11:24015.

Xu M, Wang LV (2005) Universal back-projection algorithm for photoacoustic computed tomography. *Physical review E, Statistical, nonlinear, and soft matter physics* 71:16706.

Yao J, Wang LV (2014) Sensitivity of photoacoustic microscopy. *Photoacoustics* 2:87-101.

Zouboulis CC, Jourdan E, Picardo M (2014) Acne is an inflammatory disease and alterations of sebum composition initiate acne lesions. *Journal of the European Academy of Dermatology and Venereology : JEADV* 28:527-32.

Zouboulis CC, Schagen S, Alestas T (2008) The sebocyte culture: a model to study the pathophysiology of the sebaceous gland in sebostasis, seborrhoea and acne. *Archives of dermatological research* 300:397-413.

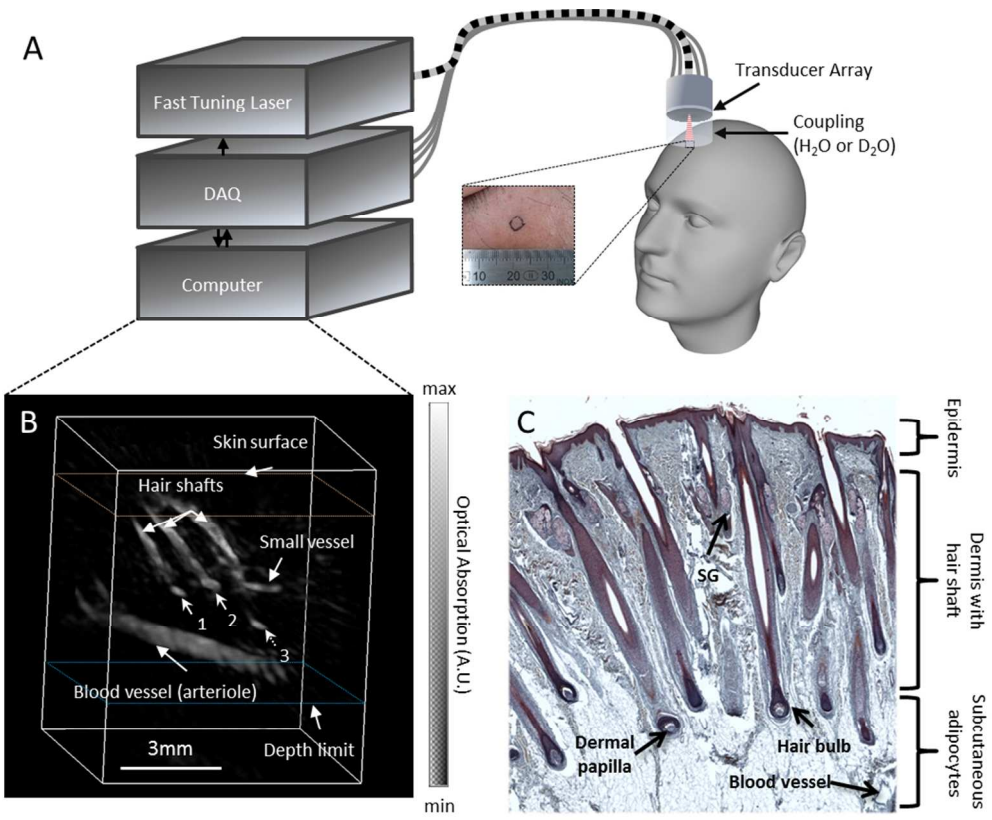

Figure 1: Handheld optoacoustic probe for high resolution real-time imaging of hair follicles. (A) Schematic of the imaging system and approach. The subject is imaged using a 512-element semi-spherical detector array that captures three-dimensional multispectral optoacoustic data in real time. The region of interest is illuminated using a pulsed OPO laser capable of fast wavelength tuning in an extended range 660-1300 nm at a rate of up to 100 Hz. The data acquisition unit (DAQ) simultaneously digitizes the optoacoustic signals, which are subsequently processed using a GPU-accelerated image reconstruction code to render 3D images for each laser shot. (B) Representative 3D optoacoustic image, demonstrating general physiological structures below the skin surface, including the hair shafts and bulbs, dermal papilla (indicated by numbered arrows), and a deeper, larger blood vessel. The dermal papilla appear to be detached in hairs marked by arrow 3, suggesting this follicle may be in the catagen or telogen phase, whereas the dermal papillae of the hairs marked by arrows 1and 2 appear to be attached, suggesting these follicles are in an anagen phase. (C) Representative Masson's Trichrome microscope image (at 10x magnification) from paraffin embedded scalp hair of a healthy individual. When compared with the optoacoustic images, it reveals similar structures, namely, the dermal papilla, hair shafts and bulbs, and a large subcutaneous blood vessel. The hair bulbs and dermal papilla are located at some places in the subcutaneous fat tissue. Note that also visible in the histological image are sebaceous glands (SG) in the dermis close to the skin surface.
372x305mm (72 x 72 DPI)

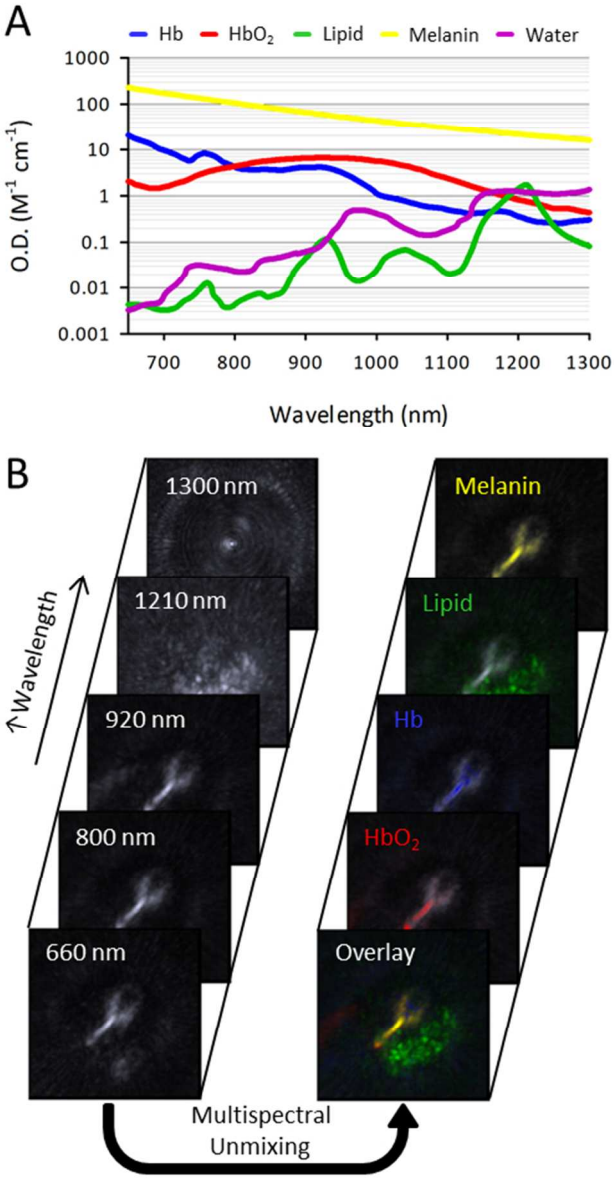

Figure 2: The multispectral imaging approach. (A) Images are collected at a range of wavelengths, chosen based on the shown absorption profiles of the chromophores of interest. (B) Optoacoustic images acquired at the multiple wavelengths allow for a linear unmixing of the data on a per-voxel basis and accurate mapping and quantification of the relative contribution of each chromophore.
185x340mm (72 x 72 DPI)

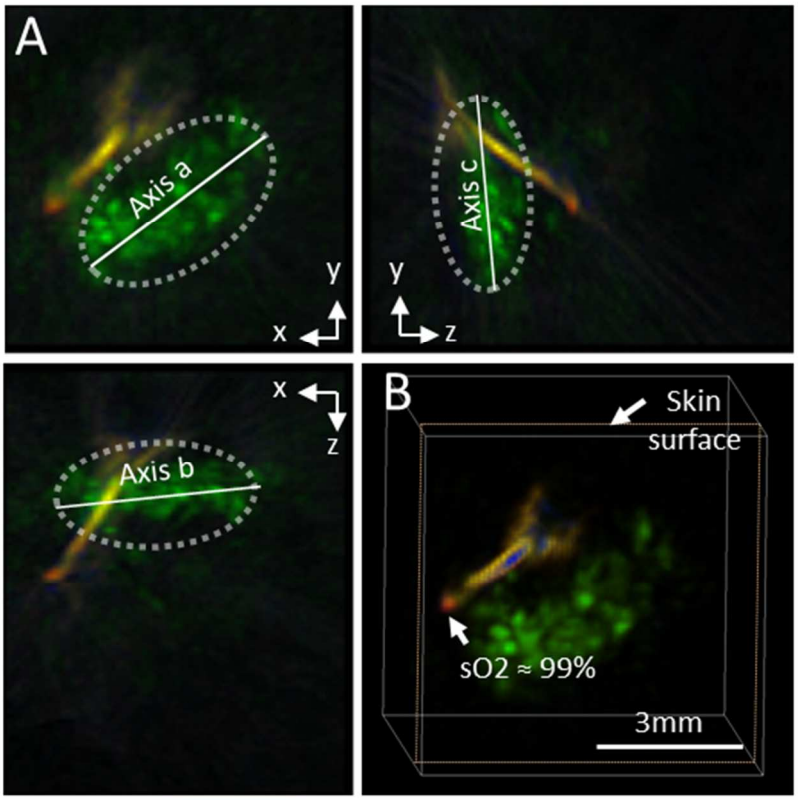

Hair Measurements

n	Length (mm)	Volume (mm^3)
1	3.21	0.285
2	3.10	0.222
3	3.20	0.326

Figure 3: Single pilosebaceous unit imaged on the forehead. (A) Unmixed images of a single hair on the scalp of a healthy volunteer. Multispectral unmixing allowed for the visualization of the single hair at depth, and also revealed an ellipsoid-like lipid structure near the follicle root. The dimensions of the lipid content were calculated along three axes shown in the orthogonal view in panel A (a = 4.3 mm, b = 2.5 mm, c = 3.4 mm). Assuming an elliptical shape, the estimated volume of the lipid structure was calculated to be 153 µL. (B) 3D representation of the unmixed data. (C) Photograph as well as a high-resolution micrograph (inlay) of the hair imaged, prior to shaving the hair. The length and volume of the hair shaft and bulb was measured from three separate scans, as quantified in the inlaid table. Of particular interest is that the follicle bulb shows a high level of oxygenation, presumably corresponding to the highly-oxygenated capillary bed feeding the follicle. Colors reflect the contribution of each of the unmixed chromophores as follows: grey – OA signal at 800 nm; blue – deoxy hemoglobin; red – oxyhemoglobin; green – lipid; yellow – melanin.
188x276mm (72 x 72 DPI)

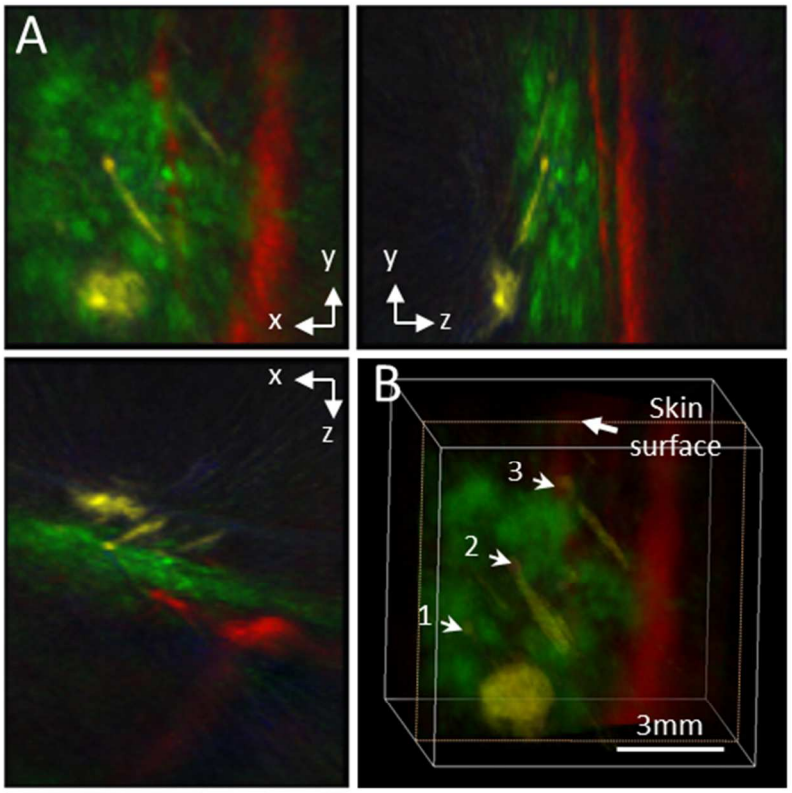

Hair Measurements

n	Length (mm)	Volume (mm^3)
1	2.25	0.127
2	2.39	0.066
3	1.93	0.073

Figure 4: A cluster of pilosebaceous units imaged on the hand. (A) The unmixed images of a hand in a region where both a mole (melanocyte deposit) and hairs are seen. The unmixed signal shows a strong lipid content, as well as strong melanin content, correlating to melanin concentrated in the hairs and mole. The lipid content was dispersed around the hairs deep under the skin surface, as can be seen in the orthogonal and 3D views of the hair. (B) Volumetric representation of the unmixed data. (C) Photograph, as well as a high-resolution micrograph (inlay) of the region, mole, and hairs imaged, after shaving the hairs. Measures of the length and volume of each of the three hairs visualized in this scan are tabulated in the inlaid table. Colors reflect the contribution of each of the unmixed chromophores as follows: grey – OA signal at 800 nm; blue – deoxy hemoglobin; red – oxyhemoglobin; green – lipid; yellow – melanin.
189x280mm (72 x 72 DPI)

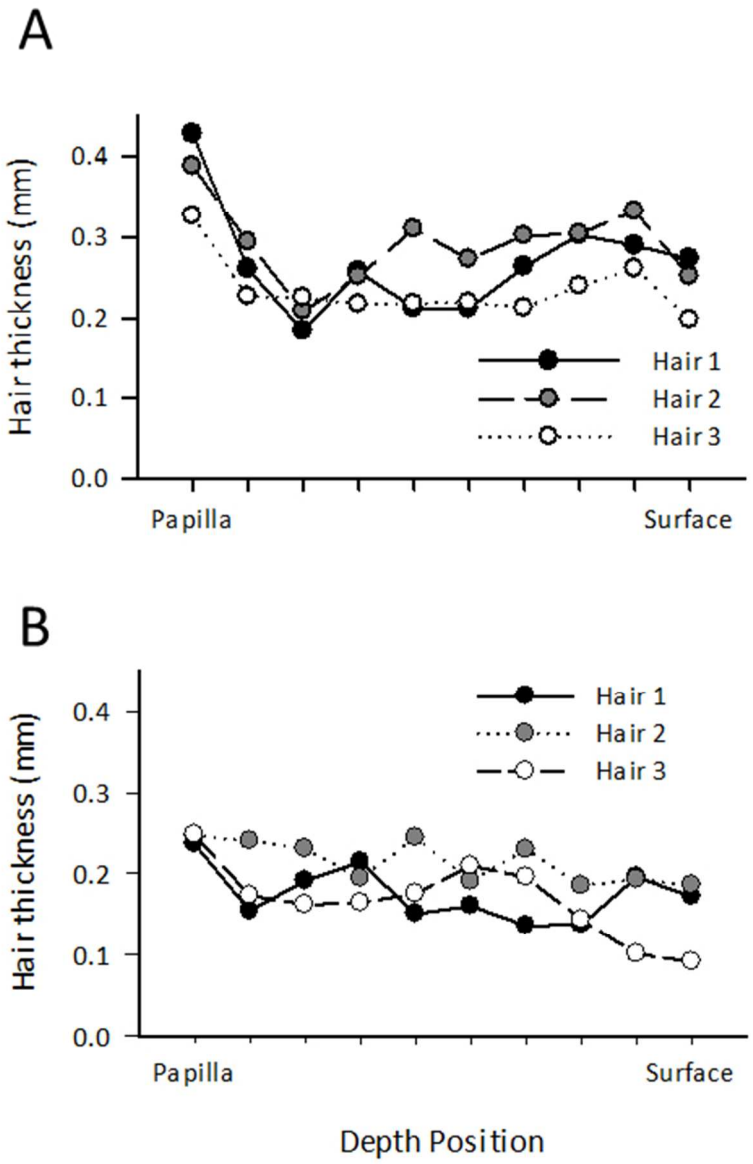

Figure 5: Measurements of hair shaft thickness at 10 different depths starting at the dermal papilla and ending at the skin surface. (A) Hair thicknesses measured on the scalp, which correspond to hairs 1, 2, and 3 of Fig 1B. (B) Hair thicknesses measured on the hand, corresponding to hairs 1, 2, and 3 of Fig 3B.
182x260mm (72 x 72 DPI)

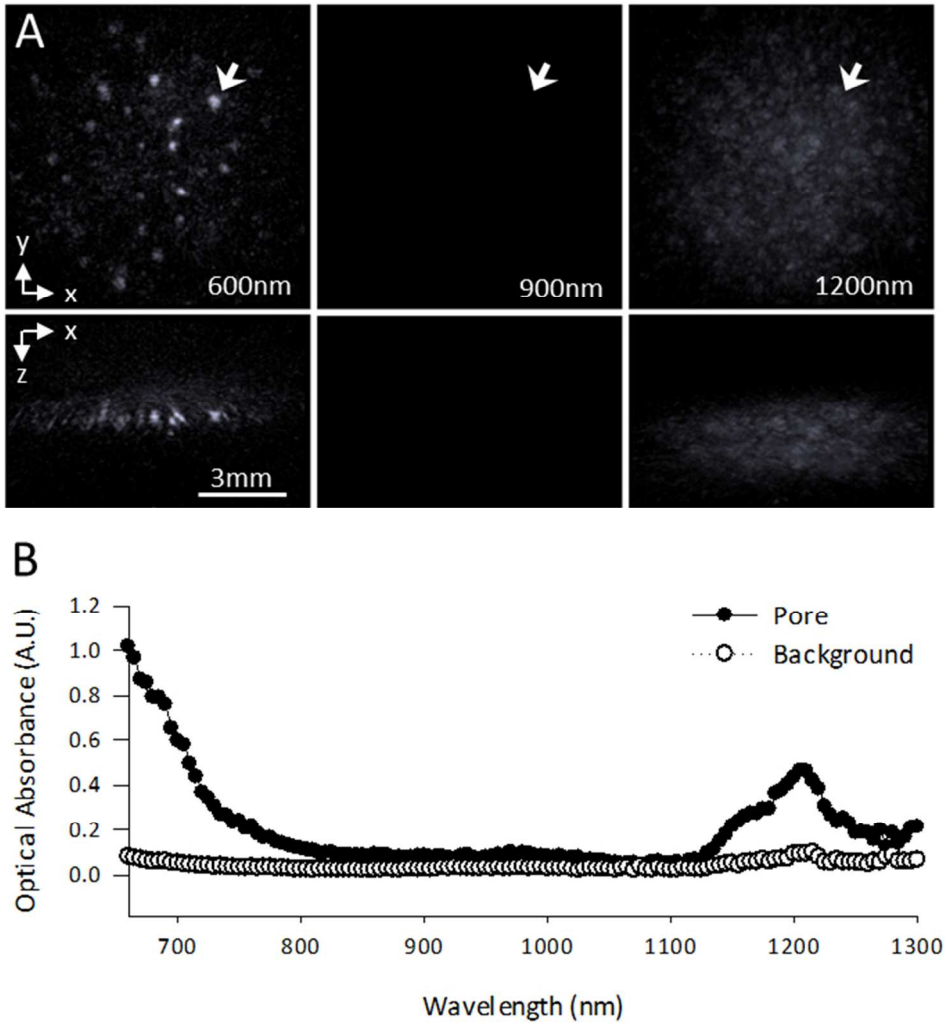

Figure 6: Multi-wavelength imaging of pigmented pores on the forehead of a volunteer. (A) Several highly-absorbing spherically-shaped objects are clearly identified near the skin surface at the shorter wavelengths, for example in image taken at 660 nm. These structures attenuate and eventually disappear at higher wavelengths. (B) The absorption spectrum of a given pore-like structure, as indicated by an arrow in panel A. This spectrum shows some similarity to the known absorbance spectra of porphyrin IX produced by the bacteria p. acnes or it could represent a mixture of microbial chromophores with sebaceous gland lipids altered by oxidation or microbial metabolism.
255x267mm (72 x 72 DPI)